AGU PUBLICATIONS

JGR

Journal of Geophysical Research: Earth Surface

RESEARCH ARTICLE
10.1002/2015JF003783

Key Points:
- Coastal dune growth and destruction can be understood using an impulsive model
- Onset of bistable behavior is controlled by storm recurrence and dune growth rate
- Modeled behaviors qualitatively match observations

Correspondence to:
E. B. Goldstein,
evan.goldstein@unc.edu

Citation:
Goldstein, E. B., and L. J. Moore (2016), Stability and bistability in a one-dimensional model of coastal foredune height, *J. Geophys. Res. Earth Surf.*, *121*, 964–977, doi:10.1002/2015JF003783.

Received 9 NOV 2015
Accepted 21 APR 2016
Accepted article online 28 APR 2016
Published online 13 MAY 2016

Stability and bistability in a one-dimensional model of coastal foredune height

Evan B. Goldstein[1] and Laura J. Moore[1]

[1]Department of Geological Sciences, University of North Carolina at Chapel Hill, Chapel Hill, North Carolina, USA

Abstract On sandy coastlines, foredunes provide protection from coastal storms, potentially sheltering low areas—including human habitat—from elevated water level and wave erosion. In this contribution we develop and explore a one-dimensional model for coastal dune height based on an impulsive differential equation. In the model, coastal foredunes continuously grow in a logistic manner as the result of a biophysical feedback and they are destroyed by recurrent storm events that are discrete in time. Modeled dunes can be in one of two states: a high "resistant-dune" state or a low "overwash-flat" state. The number of stable states (equilibrium dune heights) depends on the value of two parameters, the nondimensional storm frequency (the ratio of storm frequency to the intrinsic growth rate of dunes) and nondimensional storm magnitude (the ratio of total water level during storms to the maximum theoretical dune height). Three regions of phase space exist (1) when nondimensional storm frequency is small, a single high resistant-dune attracting state exists; (2) when both the nondimensional storm frequency and magnitude are large, there is a single overwash-flat attracting state; (3) within a defined region of phase space model dunes exhibit bistable behavior—both the resistant-dune and the low overwash-flat states are stable. Comparisons to observational studies suggest that there is evidence for each state to exist independently, the coexistence of both states (i.e., segments of barrier islands consisting of overwash-flats and segments of islands having large dunes that resist erosion by storms), as well as transitions between states.

1. Introduction

Coastal foredunes that develop along sandy coastlines protect landward habitats from elevated ocean water level. Understanding the controls on dune size, shape, and growth ultimately allows for more detailed and accurate quantitative forecasts of the impact of storms on dune-backed coasts. A large body of previous work has investigated the biophysical feedback between vegetative and sand transport processes that causes coastal foredunes to grow [e.g., *Hesp*, 1989; *Arens*, 1996; *Arens et al*., 2001; *Hesp*, 2002; *Kuriyama et al*., 2005; *McLean and Shen*, 2006; *Zarnetske et al*., 2012; *de Vries et al*., 2012; *Durán and Moore*, 2013; *Keijsers et al*., 2015]. This dune-building feedback occurs when sand is transported in the vicinity of dune-building grasses, which, acting as roughness elements, cause local reductions in wind shear stress leading to localized sand deposition [e.g., *Hesp*, 1989; *Arens*, 1996; *Kuriyama et al*., 2005]. The resulting burial of dune-building grasses, in turn, stimulates grass growth [e.g., *Maun and Perumal*, 1999] further enhancing deposition ultimately giving rise to dunes. Recently, *Houser et al*. [2015] provided evidence (new observations and reanalysis of data found in the literature) indicating that the vertical growth of coastal foredunes exhibits logistic behavior for the low (~2 m) dunes along the U.S. Gulf Coast.

Storm events interrupt the growth of coastal dunes and cause erosion. Predicting dune erosion has been the focus of recent numerical modeling efforts, using methods ranging from process-based numerical models [e.g., *McCall et al*., 2010] to empirical techniques [e.g., *Long et al*., 2014]. These models focus on developing predictions for a single storm event, but dune morphology is controlled by sequences of storm events through repeating cycles of dune growth and dune destruction [e.g., *Hesp*, 2002; *McLean and Shen*, 2006; *Claudino-Sales et al*., 2008; *Houser and Hamilton*, 2009; *Keijsers et al*., 2014; *Durán and Moore*, 2015]. Understanding the consequences of repeated storm events on dune morphology is especially salient because storms are predicted to increase in intensity (and potentially, frequency) as climate changes [e.g., *Emanuel*, 2013]. Additionally, future storm surge and wave runup will be superimposed on rising mean sea level [*Intergovernmental Panel on Climate Change*, 2014], which increases the impact of storm events [e.g., *Tebaldi et al*., 2012].

These two processes, dune growth arising from the biophysical feedback and storm-driven dune destruction, must be combined to develop a mechanistic understanding of the temporal evolution of dunes subject to

repeat storm events. Based on numerical experiments conducted using a spatially explicit model of vegetated coastal foredunes, *Durán and Moore* [2015] suggest that under certain conditions, the interplay of these two processes leads to island bistability—the tendency for islands to exist in one of two alternate stable states (i.e., equilibrium elevations). This finding is supported by a bimodal distribution of observed foredune elevations from the Virginia Barrier Islands, USA [*Durán and Moore*, 2015]. Multiple stable states have been observed in the fixed versus active state of sand dunes [*Yizahq et al*., 2007, 2009; *Kinast et al*., 2013; *Bel and Ashkenazy*, 2014] as well as other ecogeomorphic systems [e.g., *Fagherazzi et al*., 2006; *Coco et al*., 2006; *Heffernan*, 2008; *Marani et al*., 2010; *Carr et al*., 2010].

Here we further the investigation of coastal foredunes by developing a simplified, one-dimensional nonlinear model of foredunes under periodic storm events, a complementary approach that allows us to explore the stability of coastal foredune height for a reduced parameter space and therefore gain additional insights into dune and island dynamics. Work presented here is a simplification of the three-dimensional nature of coastal dunes and does not address complications such as nonstationary coastlines where foredunes change cross-shore position following a storm—this work is focused on dune erosion that is followed by "in place rebuilding" (in the sense of *Hesp* [2002]). Our goal is to address the behavior of coastal dunes at the multiple-storm timescale. We develop the model from observations of the U.S. East and Gulf Coasts, and therefore, the results are most relevant in sandy, low-slope settings where foredunes are less than ~5 m in height. The model presented in this contribution is exploratory [e.g., *Murray*, 2003], intended for investigation (using a reduced set of variables) of the dynamics of coastal foredunes on stationary coastlines.

2. Model Structure

The model is composed of two pieces, the growth of coastal dunes by coupled aeolian-vegetative processes and the destruction of dunes by storm events. The simplified mathematical treatment of these processes and the combined model follow here.

2.1. Logistic Growth

Observations presented in *Houser et al*. [2015] demonstrate that the growth of coastal foredunes can be successfully described by the Verhulst logistic equation [*Verhulst*, 1838]:

$$\frac{dD}{dt} = rD\left(1 - \frac{D}{D_{max}}\right), \tag{1}$$

where D is the height of the sand surface where a coastal foredune is present or would be present (hereinafter referred to as dune height) [L], t is time [T], r is the intrinsic growth rate [1/T], and D_{max} is the maximum theoretical dune height [L]. The logistic growth/recovery of dunes after storm events has been described physically by *Morton et al*. [1994] and *Houser et al*. [2015] and incorporated into simulations of dune growth by *Durán and Moore* [2015]—the dune growth process is observed and simulated to begin slowly as sand returns to the beach and accumulates via aeolian transport, building the elevation of the back beach to a critical elevation above which plants can (re)establish because inundation and overwash are sufficiently infrequent. Once vegetation becomes established and if sufficient mobile sand is present, dune growth can then occur more rapidly as wind blows sand to the newly vegetated back beach and the dune-building feedback is initiated. Dune growth eventually slows as the dune approaches its theoretical maximum height, D_{max}.

We assume r and D_{max} are time invariant parameters. Previous work can help to constrain realistic values for the two free parameters r and D_{max}. From observations of dune growth *Houser et al*. [2015] present values for the growth parameter ranging from $0.05 \leq r \leq 0.55$. The intrinsic growth rate, r, encapsulates several environmental properties. For example, model results presented in *Durán and Moore* [2013] show that foredune formation time, analogous to $1/r$, scales with three factors: (1) the minimum distance from the shoreline for plants to survive long enough to build a foredune (L_{veg}); (2) the average wind speed during transport events; and (3) the inverse of sand flux from the beach to the dune (which incorporates the fraction of time when transport occurs). Additional factors include (but are not limited to) foredune vegetation growth rates [e.g., *Hesp*, 2004], climate controls on vegetation cover [e.g., *Ryu and Sherman*, 2014], wind directionality [e.g., *Bauer et al*., 2012], and sediment supply effects [e.g., *Bauer and Davidson-Arnott*, 2002].

Previous work has shown that vegetation morphology controls D_{max}—plants that produce more vertical rhizomes, longer vertical rhizomes, or more/longer tillers will tend to produce taller dunes compared to plants with a more lateral growth form [e.g., *Hesp*, 2004; *Zarnetske et al*., 2012; *Hacker et al*., 2012]. Model results presented in *Durán and Moore* [2013] find that all other factors being equal, maximum foredune height (D_{max}) scales with L_{veg}, with secondary contributions from wind speed.

2.2. Storm Erosion

We use empirical data to derive a smooth relationship for dune erosion by storms. *Long et al*. [2014] compiled observational data of coastal dune height before and after four large storm events along the U.S. East and Gulf Coasts. By comparing dune height change with parameters from storm forcing conditions and hydrodynamic simulations of the storm events, *Long et al*. [2014] developed several piecewise functions to relate dune erosion to nearshore hydrodynamic characteristics of the storm event. The data yield basic insight into vertical dune erosion—vertical erosion is minimal or nonexistent when water level does not overtop the dune. After overtopping, vertical erosion occurs and generally increases as a function of water level. At ever higher water level, large scatter and/or potentially negative trends occur, which *Long et al*. [2014] speculate may be caused by spatial processes (such as a water surface gradient between the bay and ocean) during severe storms. Additional observations will resolve the causative mechanism of this trend.

We use the data compiled by *Long et al*. [2014] to develop a single smooth nonlinear function to relate dune erosion to the total water level during a storm event. Specifically, we relate change in dune elevation normalized by the prestorm dune height ($\Delta D/D$) to the total water level normalized by the prestorm dune height (R/D, where R [L] is the total water level measured from the same datum as D). We develop this new equation by analyzing the data collected by *Long et al*. [2014] using a machine learning algorithm [*Schmidt and Lipson*, 2009, 2014]. The algorithm is based on genetic programming [*Koza*, 1992], in which a population of randomly generated initial candidate solutions is adjusted through evolutionary processes (i.e., crossover and mutation) to develop smooth solutions of the form $\left(\frac{\Delta D}{D}\right) = f(R/D)$. The arrangement and value of constants, variables and mathematical operators are modified at each time step to develop candidate solutions (equations) that can reproduce the relationships present in the data. This technique has been used successfully in other coastal studies, [*Goldstein et al*., 2014, 2013; *Limber et al*., 2014; *Tinoco et al*., 2015] and we refer the reader to these works and the initial work by *Schmidt and Lipson* [2009] for additional details of the technique.

To analyze the data using the machine learning algorithm, we split the data from *Long et al*. [2014] in half randomly. One half is used as training data ($n = 83$), while the other half is retained as testing data ($n = 84$) and is not shown to the genetic programming routine. A central issue of machine learning and any empirical/inductive method is the behavior of the derived function outside the range of data. To prevent behavior that is not physically reasonable, we add additional data points to the training data to act as constraints. Specifically, we add data to mandate that dune erosion collapses to 0 when R/D is small (i.e., when the dune is large and/or the total water level is low; $\frac{\Delta D}{D} \rightarrow 0$ when $\frac{R}{D} \rightarrow 0$).

The training data (and added constraints) are passed through the machine learning technique to yield a smooth predictor of dune erosion during storms. However, the solution to the genetic programming routine is not a single equation but rather a set of equations with increasing size (complexity) and decreasing error (here we use mean squared error). We use the "last cliff" technique, suggested by *Schmidt and Lipson* [2009], to pick a solution that balances complexity and error reduction. The resulting predictor is

$$\frac{\Delta D}{D} = \frac{\frac{R}{D}}{C_1 + \left(\left(\frac{R}{D}\right)\left(\frac{R}{D} - C_2\right)\right)}, \tag{2}$$

where ΔD is the reduction in dune height as a result of the storm [L], R is the total water level height [L] measured from the same datum as D, and C_1 and C_2 are (dimensionless) empirical parameters set to 8.8 and 4.6, respectively. Figure 1 shows the solution compared to the data from *Long et al*. [2014].

There are several aspects of this newly developed curve that are important to note. First the data from *Long et al*. [2014] contain a significant amount of scatter (Figure 1). This is the result of the simplified nature of the functional relationship. For instance, we use only a single hydrodynamic constraint: the maximum total water level (R) during the storm event. In their analysis *Long et al*. [2014] were able to reduce the

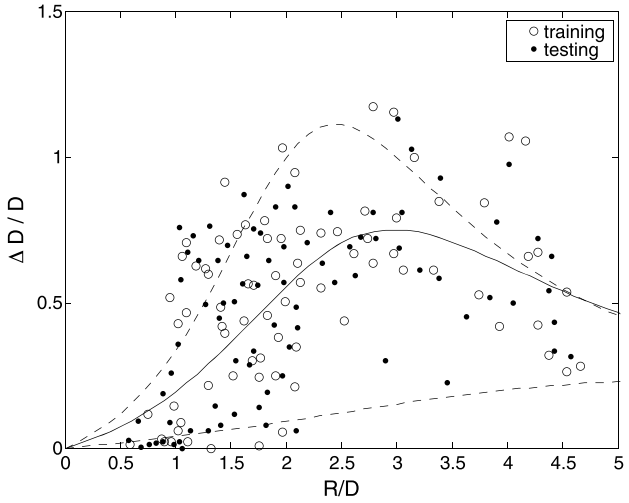

Figure 1. Black dots show the data collected by *Long et al*. [2014]—change in elevation normalized by the prestorm dune height ($\Delta D/D$) versus the total water level relative to the prestorm dune height (R/D). Data have been divided in half into training (open) and testing data (filled). The black line is the fit from equation (2). Black dashed lines represent an upper and lower envelope for the data that we use to address the sensitivity of the model.

dispersion of data by including swash excursion as a second hydrodynamic parameter. We do not include swash here because adding this extra parameter would result in an increase in degrees of freedom and therefore an additional parameter to constrain. It is likely that significant scatter also exists in the data set of *Long et al*. [2014] because storm duration is not included; we do not know of a data set comparable to that of *Long et al*. [2014], which incorporates storm duration. Furthermore, including storm duration in the predictor would, as in the case of including the swash excursion, require us to constrain an additional parameter, increasing the degrees of freedom, and detracting from our simplified approach.

The developed curve fit using machine learning does not perfectly fit the data —$\frac{\Delta D}{D}$ tends to be over predicted for $\frac{R}{D}$ values less than 0.5 and $\frac{\Delta D}{D}$ tends to be under predicted for $\frac{R}{D}$ values greater than 0.5 (Figure 2). We can address the scatter of the data and the poor prediction of our single optimized curve by adjusting C_1 and C_2 in (2) to fit the upper and lower values of the *Long et al*. [2014] data set (Figure 1). The curve delineating the upper envelope of the data overpredicts dune erosion during storms, whereas the curve delineating the lower envelope under predicts dune erosion during storms (Figure 2). In the results (section 3.1) we include analysis of model results with adjusted values of C_1 and C_2 and show that the qualitative behavior of this model is independent of model parameterization.

The relative total water level (R/D) represents the total water level normalized by the prestorm dune height, so when $R/D < 1$ the water level during a storm is below the dune (the collision regime of *Sallenger* [2000]) and when $R/D > 1$ water level during a storm is above the dune (overwash or inundation regime of *Sallenger* [2000]). Note in Figure 1 that the change in dune height $\left(\frac{\Delta D}{D}\right)$ is near zero when $R/D<1$ (the collision regime) and decays to 0 as $\frac{R}{D} \rightarrow 0$. Thus, the *Long et al*. [2014] data set, and the curve we developed from it as described above, captures the empirical finding that when water level is lower than dune crest height, vertical dune erosion may occur but is generally minor (for instance, when collision produces slumping) [e.g., *Palmsten and Holman*, 2011]. This applies even in the case of high dunes (e.g., 10s of meters) impacted by large storm

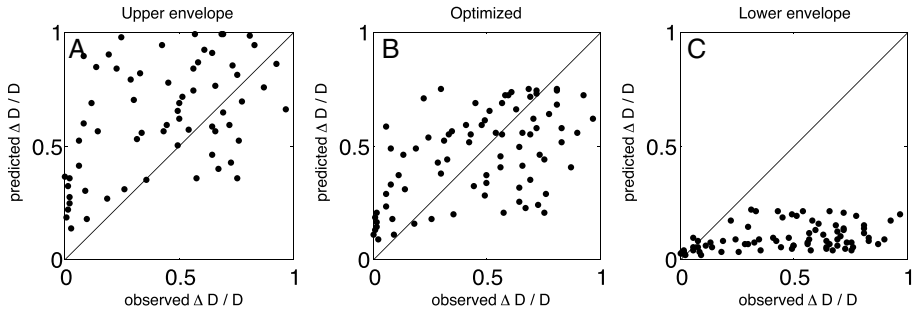

Figure 2. Observed dune erosion versus predicted dune erosion using only the testing data for equation (2). (a) The upper envelope of the data (over-prediction of erosion), (b) the optimized values, and (c) the lower envelope (under prediction of erosion).

events that produce large total water levels (e.g., several meters), which are parameterized on this curve as $R/D < 1$, yielding minor vertical dune erosion.

We include a threshold version of equation (2) in the results (section 3.2) to explore the effect of limiting vertical dune erosion solely to times when water level is above the dune height. In this version of the model formulation we set dune erosion $\left(\frac{\Delta D}{D}\right)$ to zero in the collision regime, when the total water level does not breach the prestorm dune crest ($R/D < 1$). When $R/D \geq 1$ we use the machine learning-derived erosion rule. We have also tried versions of the erosion rule in which erosion is set to a single value when $R/D \geq 1$ or increases linearly to a given value when $R/D \geq 1$ (i.e., there is no erosion maxima in contrast to what is shown in Figure 1). These model results are indistinguishable from the threshold model presented in section 3.2. Our goal in presenting and discussing these variations on the erosion rule is to communicate that the model result (i.e., bistability) is not dependent on any one specific erosion rule or the local maxima in erosion found by *Long et al.* [2014].

2.3. Storm Climatology

Compared to the slow logistic growth of dunes, the erosion of dunes by storms is an impulsive process (i.e., an "impulse") because it occurs at discrete times. As such (2) operates at discrete moments. Because our goal is to put forward a simplified, exploratory model to maximize insights into the basic process, we simplify the storm climatology and assume a single "characteristic" storm event occurs at a constant storm frequency S [1/t] with a constant magnitude (total water level height) of R [L]. This is, admittedly, a substantial simplification of the probabilistic nature of storm occurrence. In future work we aim to relax this assumption and couple this simplified framework to a probabilistic treatment of total water level [e.g., *Serafin and Ruggiero*, 2014].

2.4. Combined Model and Nondimensionalization

Together (1) and (2) yield a single model for dune growth and destruction. This model is an impulsive differential equation [e.g., *Bainov and Simeonov*, 1993; *Tang and Chen*, 2002] in which dune growth (1) operates continuously (at all times) while dune destruction (2) is an impulse, operating instantaneously (at discrete times). Nondimensionalizing (1) and (2), where $D^* = \frac{D}{D_{\max}}$, $t^* = rt$, and $R^* = \frac{R}{D_{\max}}$, and solving the logistic equation yields the equation set:

$$D^* = \frac{D_0^*}{D_0^* + \left(1 - D_0^*\right)e^{-t^*}} \tag{3a}$$

$$\Delta D^* = \frac{R^*}{C_1 + \left(\left(\frac{R^*}{D^*}\right)\left(\frac{R^*}{D^*} - C_2\right)\right)}, \tag{3b}$$

where D_0^* is the initial value of D^*. We refer to D^* as the nondimensional dune height and R^* as the nondimensional total water level. The discrete equation (3b) operates at time intervals defined by the storm period $\left({}^1/_S\right)$. The nondimensional storm period when the impulse operates is therefore ${}^1/_{S^*}$ where $S^* = {}^S/_r$. We refer to S^* as the nondimensional storm frequency (the ratio between storm frequency and the intrinsic growth rate of the dune).

To explore the solution of the combined impulsive differential equation model we combine ((3a) and (3b)) into a single one-dimensional difference equation (a stroboscopic map) which permits the analysis of nondimensional dune height (D^*) at the storm period $\left({}^1/_{S^*}\right)$—after continuous growth and a single storm event. By definition (3b) represents the vertical erosion of the dune from a single storm event and

$$\Delta D^* = D^{*-} - D^{*+}, \tag{4}$$

where D^{*-} is the dune height immediately before the storm and D^{*+} is the dune height immediately after the storm. The (immediately) prestorm dune height, D^{*-}, is (3a) taken after a period of growth (with a duration of the nondimensional storm period; ${}^1/_{S^*}$):

$$D^{*-} = \frac{D_{t^*}^*}{D_{t^*}^* + \left(1 - D_{t^*}^*\right)e^{-\frac{1}{S^*}}}, \tag{5}$$

where $D_{t^*}^*$ is the dune height at the beginning of the interstorm interval (i.e., immediately following the previous storm).

Storm erosion (ΔD^*) is dependent on the dune height immediately before the current storm (D^{*-}). Substituting (5) into (3b) yields

$$\Delta D^* = \frac{R^*}{C_1 + \left(\left(\frac{R^*}{D^{*-}}\right)\left(\frac{R^*}{D^{*-}} - C_2\right)\right)}. \tag{6}$$

Substituting (5) and (6) into (4), and rearranging, yields the nondimensional dune height immediately after the storm event:

$$D^{*+} = D^{*-} - \frac{R^*}{C_1 + \left(\left(\frac{R^*}{D^{*-}}\right)\left(\frac{R^*}{D^{*-}} - C_2\right)\right)}. \tag{7}$$

Formally D^{*+} is $D^*_{t^*+\frac{1}{S^*}}$, the dune height after an interval of $\frac{1}{S^*}$ (during which continuous growth and a single storm have occurred). The complete model is therefore

$$D^*_{t^*+\frac{1}{S^*}} = f\left(D^*_{t^*}\right) - \frac{R^*}{C_1 + \left(\left(\frac{R^*}{f\left(D^*_{t^*}\right)}\right)\left(\frac{R^*}{f\left(D^*_{t^*}\right)} - C_2\right)\right)}, \tag{8}$$

where

$$f\left(D^*_{t^*}\right) = \frac{D^*_{t^*}}{D^*_{t^*} + \left(1 - D^*_{t^*}\right)e^{-\frac{1}{S^*}}}. \tag{9}$$

3. Model Results

3.1. Basic Formulation

Stable equilibrium dune heights (i.e., stable attracting states) occur when dune growth during interstorm periods is offset, or balanced, by dune erosion during storm events. This condition occurs when the post storm dune height is invariant in time; $D^*_{t^*+\frac{1}{S^*}} = D^*_{t^*}$. We solve (8) numerically in time for a range of initial conditions $\left(0 \le D^*_{t^*} \le 1\right)$ to determine the number of stable attracting states. The numerical routine calculates the poststorm dune height, at a single station, as continuous dune growth interspersed with discrete storm events. By looking at dune height across the timescale of multiples storms (i.e., the height that poststorm dune height converges to over long time scales) we can examine the stable states predicted by the model.

The stability diagram, Figure 3a, highlights the number of unique stable states in each region of S^*-R^* parameter space (i.e., the nondimensional parameter space that is equivalent to storm frequency-magnitude). Convergence to an attracting state occurs for all values of S^* and R^* used in this study. Three prominent regions exist on the stability diagram (Figure 3a). First, when nondimensional storm frequency S^* is low (representing infrequent storms or fast growing dunes), all model results converge to a single attracting dune height, regardless of nondimensional total water level (R^*). Second, when S^* is large (representing frequent storms or slow dune growth) and R^* is large (representing high storm water level or a low maximum dune height), a single attracting state exists. Third, if S^* is moderate but R^* remains low (representing low storm water level or a large maximum dune height), two attracting states exist; this is the bistable region of the model.

Bifurcation diagrams along lines of equal R^* are shown in Figures 3b–3d to examine the equilibrium nondimensional dune height of these attracting states. Figures 3b–3d contain three regions that correspond to the three regions of the stability diagram (Figure 3a). The regions in the bifurcation diagrams are differentiated by the number of stable states that exist at each value of S^*: First, when storms are less frequent relative to the dune growth parameter (low S^*), there exists only a single, stable nondimensional dune height that is greater than $D^* = 0.5$. We refer to this as the "resistant-dune" state. Second, when storms are more frequent relative to the intrinsic growth rate of dunes (high S^*) there exists only a single stable dune height near $D^* = 0$. We refer to this as the "overwash-flat" state. Third, at moderate nondimensional storm frequency (S^*), there is a bistable region in which both states (resistant-dunes and overwash-flat) occur and are stable.

Note that model results are nondimensional and the absolute height of each dune state (high and low) is relative to D_{max}, which is a local factor. However, because this model is built using a growth equation and storm destruction equation both parameterized along the US East and Gulf Coast, it is reasonable to assign

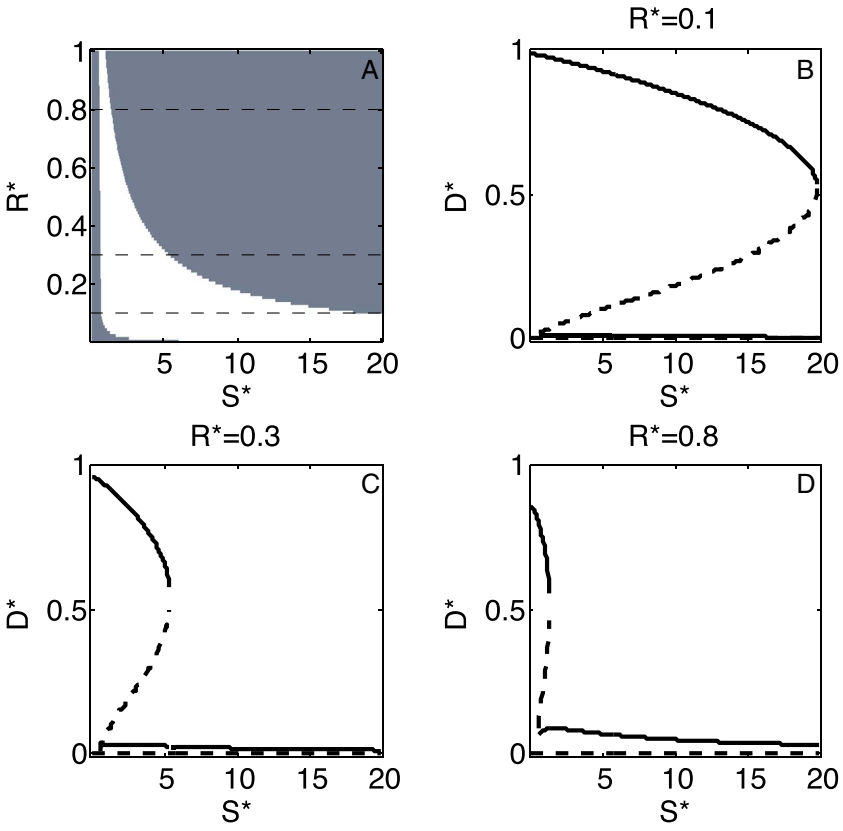

Figure 3. (a) Stability diagram in S^*-R^* parameter space using equation (8). Grey regions contain a single attracting state. The bistable region is shown in white. Horizontal dotted lines in Figure 3a show the location of the bifurcation diagrams (b–d). (b) Bifurcation diagram at $R^* = 0.1$. Solid lines are the location of stable fixed points, dotted lines are unstable fixed point location (i.e., the separatrix). (c) Bifurcation diagram $R^* = 0.3$. (d) Bifurcation diagram $R^* = 0.8$.

rough values of $D_{max} = 2$–5 m, which suggests a range for the resistant-dune state of ~1–5 m and a range of values for the overwash-flat state from 0.1 m to 1 m.

In the bistable region, the initial dune height controls whether a dune will grow or decay as it evolves toward one of the stable attracting states (Figure 3). Dunes that are above the value of the unstable fixed point—the separatrix, or the value of D^* that separates the basin of attraction for each stable state—will tend to grow, evolving toward the resistant-dune attracting state because the growth of dunes outpaces the dune erosion from periodic storms. Dunes below the value of the unstable fixed point (i.e., below the separatrix) will tend to decrease in height (evolve toward the overwash-flat state) because erosion from periodic storm events outpaces the growth of the dune.

We vary the storm erosion parameters (C_1 and C_2) in (8) to address whether or not bistability exists only as a result of model parameterization. We modify the coefficients in (2) to fit the lower limit and upper limit of the data from *Long et al.* [2014]. Functions using these new coefficients are shown in Figure 4. The lower envelope of the data, fit using $C_1 = 32$ and $C_2 = 7$ represents the case in which erosion during a storm is minimized. The upper envelope of the data, fit using $C_1 = 6$ and $C_2 = 4$ represents the case in which erosion during a storm is maximized. Using this upper envelope parameterization also leads to the potential for dune heights to be eroded below $D^* = 0$. In those cases D^* is set to 0.01. Substituting these new coefficients in (2), we again solve numerically and develop stability diagrams (Figure 4).

The stability diagrams for the upper and lower limit, compared with the stability diagram for the originally derived equation (Figure 4) are qualitatively similar. Using the upper bounds of the *Long et al.* [2014] data the bistable region expands to areas of lower nondimensional storm frequency (S^*). In addition, the single low overwash-flat state also expands to areas of lower nondimensional storm frequency (S^*) (Figure 4a). The first of these changes occurs because using the upper bounds of the *Long et al.* [2014] data exaggerates

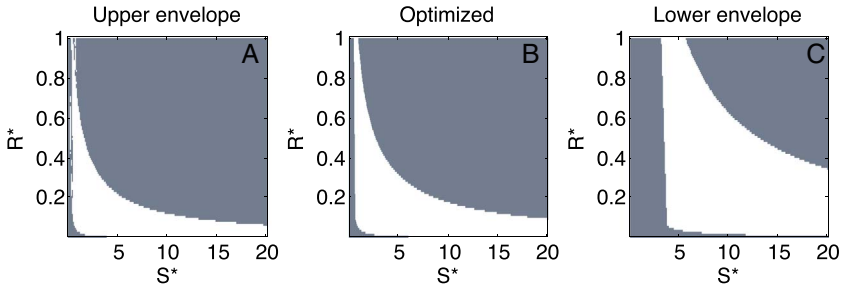

Figure 4. Stability diagram in S^*-R^* parameter space for varying coefficients in equation (2). Grey regions contain a single attracting state. The bistable region is shown in white. (a) The upper bound, (c) the lower bound, (b) the optimized equation (as in Figure 3a but shown here for side-by-side comparison).

erosion for a given storm event. The opposite is true for the curve representing the lower bound, where onset of the bistable region occurs at a higher nondimensional storm frequency S^*. Additionally, because dune erosion is minimized, the single low overwash-flat state only appears at a higher nondimensional storm frequency (S^*) (Figure 4c). The results of this analysis demonstrate that the boundaries between the regions of phase space may shift as coefficients change, but a bistable region of phase space exists regardless of the parameter values chosen.

3.2. Threshold Formulation

Figure 1 and equation (2) show that vertical dune erosion decreases to 0 as the total water level decreases. However, (2) indicates that vertical dune erosion does occur even when the water level is below the dune crest. We evaluate an alternate formulation of the model—which we discussed in section 2.2—where dune erosion follows (2) if the total water level is higher than the dune crest, but dune erosion is zero if total water level is below the dune crest (i.e., $\Delta D^* = 0$ if $\frac{R^*}{D^*_{\infty}} < 1$). We refer to the threshold where $\frac{R^*}{D^*_{\infty}} = 1$ as the overwash threshold, the boundary between the "collision" and "overwash" regime of *Sallenger* [2000]. The stability diagram for this model formulation is shown in Figure 5. In the threshold model a resistant-dune state (at the maximum theoretical dune height $D^* = 1$) is persistent throughout the range of parameter space (Figure 5). As a result, the Heaviside formulation contains only two regions of phase space: (1) a region where there is a single resistant-dune state and (2) a bistable region with both a resistant-dune and overwash-flat state. This occurs because dune erosion does not occur during storms if the dune elevation is above the height of the total water level ($\frac{R^*}{D^*_{\infty}} < 1$). As a result, dunes above the total water level always grow to the maximum height possible and the resistant-dune state is always located at $D^* = 1$. Thus, the bistable region expands greatly, encompassing the entire region of large R^* and large S^*. This is different than the basic model results presented in section 3.1 (Figure 3). In the basic model the resistant-dune state occurs at $D^* < 1$ (because erosion occurs regardless of dune height) and an increase in nondimensional storm frequency (S^*) results in the disappearance of the resistant-dune state.

The separatrix of the threshold model also has different dynamics. In the limit of very large S^*, any dune that starts above the total water level of the characteristic storm evolves toward a resistant-dune state ($D^* = 1$) because it is above the threshold for dune erosion and therefore is not eroded. When D^* starts below R^*, the dune is eroded to the overwash-flat state. As S^* decreases, the separatrix also decreases; dunes below the overwash threshold ($\frac{R^*}{D^*_{\infty}} = 1$) have sufficient time between storms to grow above the overwash threshold.

3.3. Temporal Behavior

We now show the results of the model as a time series, which reflects model behavior discretized at a timescale finer than the storm period. Results for the basic model (section 3.1) for $R^* = 0.2$ and $S^* = 3$ demonstrate model behavior in the bistable region (Figure 6a). Note that all dunes show periods of growth and erosion. However, trajectories that start above the separatrix ($D^* = 0.13$) evolve toward the resistant-dune state as growth outpaces erosion. Conversely, trajectories below the separatrix evolve toward the overwash-flat state where storm erosion outpaces dune growth. These results are comparable to those from the threshold model (section 3.2, Figure 6b) except that in the latter, dunes above the overwash threshold ($\frac{R^*}{D^*_{\infty}} = 1$) do not erode during storm events.

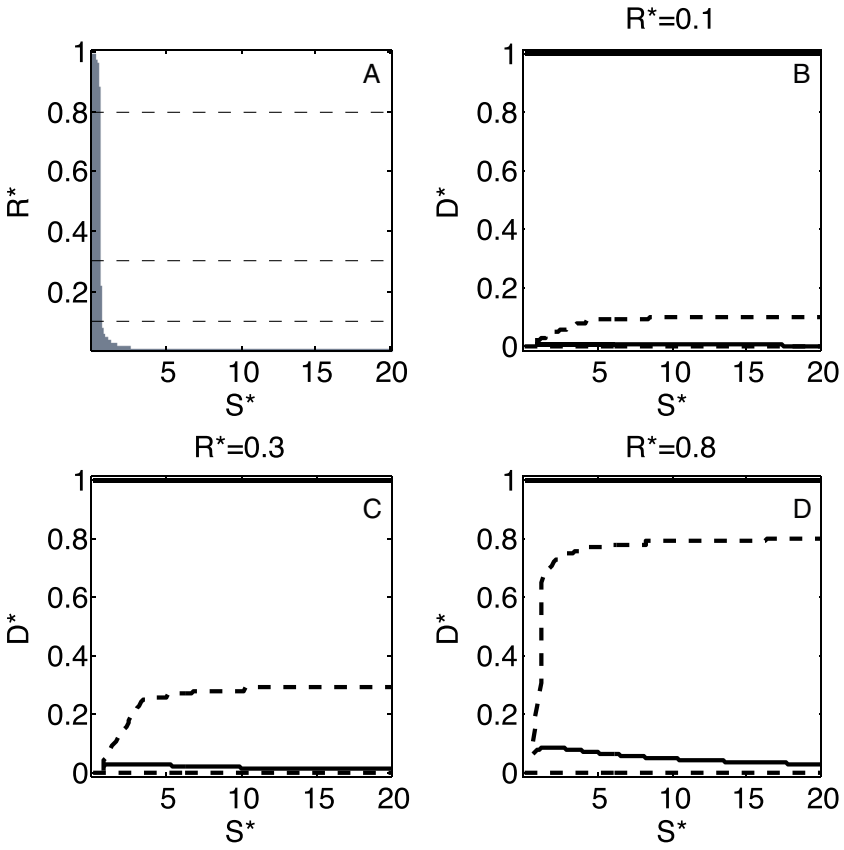

Figure 5. (a) Stability diagram in S^*-R^* parameter space using a Heaviside version of equation (2). Grey regions contain a single attracting state. The bistable region is shown in white. Horizontal dotted lines in Figure 5a show the location of the bifurcation diagrams (b–d). (b) Bifurcation diagram at $R^* = 0.1$. Solid lines are the location of stable fixed points, dotted lines are unstable fixed point location (i.e., the separatrix). (c) Bifurcation diagram $R^* = 0.3$. (d) Bifurcation diagram $R^* = 0.8$.

The behavior of model trajectories near the bifurcation point also deserves attention because of the potential for critical phenomena (such as critical slowing down) [e.g., *Scheffer et al*., 2009]. Both the basic and threshold models show a fold (or saddle node) bifurcation that relies almost entirely on variations in S^* (Figures 3–5)—an increase in storm frequency and/or a decrease in intrinsic growth rate of the dune results in bistability. Near the onset of this bifurcation, when S^* is not quite at the critical value to cause bistability (e.g., $S^* \cong 0.68$ in Figure 7), trajectories in time are significantly modified in that dune height spends an increasingly longer time in a transient state (i.e., not at the stable attracting states). We can understand this modulation using a thought experiment: If the storm frequency is held constant, but the intrinsic dune growth rate decreases, then less dune growth will occur during interstorm times. Because less dune growth occurs, the dune will take a longer time to reach a stable state (compared to a larger intrinsic growth rate). This critical phenomenon close to the onset of bifurcation, a "bottleneck," is the result of the impending bifurcation (i.e., the "ghost" of the bifurcation) [*Strogatz*, 2001]. The amount of time spent in the bottleneck increases as the bifurcation becomes closer in S^*-R^* parameter space (the square root scaling law) [*Strogatz*, 2001]. As a result, behavior is significantly modulated even before the bifurcation is reached and bistability occurs—transient dune heights become more common. Interestingly, this means that the impending bifurcation may be observable before the actual bifurcation occurs. In the context of this model, for example, this means that an overwash-flat or intermediate dune height could be a long-lived transient feature, even though the stable state of the system is the resistant-dune attracting state.

4. Discussion

4.1. Model Behavior

Stable attracting states of dune height (i.e., the high resistant-dune and the low overwash-flat attracting states) appear when dune growth during interstorm time periods is balanced by erosion during the storm

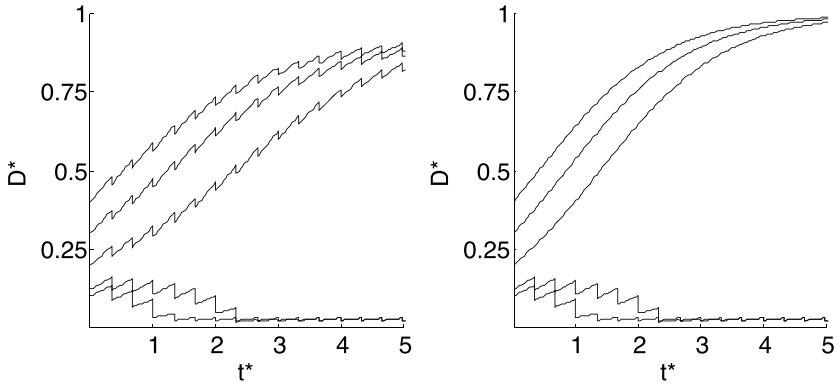

Figure 6. Nondimensional dune height time series in the bistable region, at $R^* = 0.2$ and $S^* = 3$ for initial dune heights ranging from 0 to 1 using (a) the basic model and (b) the threshold model. The saw tooth pattern is a result of the confluence of continuous dune growth and discrete times of dune erosion by storms. Model trajectories converge to the two attracting states, the resistant-dune and overwash-flat.

impulse. Within a region of S^*-R^* parameter space, the dune system exhibits two stable attracting states and a region of bistability. The behavior of the model remains unchanged when the value of the two empirical parameters in (2) is adjusted (to fit the upper and lower envelope of the data), when the storm erosion formulation is modified to explicitly incorporate an overwash threshold for dune erosion, or when the storm erosion formulation is adjusted to yield constant erosion with increasing total water level (instead of the negative dependence observed by *Long et al*. [2014]).

The appearance of bistability in this one-dimensional model is consistent with spatially explicit model results of *Durán and Moore* [2015]. Using a coupled ecomorphodynamic model that resolves wind flow, aeolian sand flux, vegetation growth dynamics, and storm erosion as a result of scarping, overwash, and inundation, *Durán and Moore* [2015] demonstrate that foredunes exhibit bistable dynamics when impinged upon by storm events (driven using a probabilistic scheme). The model presented here is built using a more coarse-grained description of the system (two empirical expressions versus many process rules and mechanistic equations) yet it is able to achieve quantitatively similar results. For example, Figure 3e presented in *Durán and Moore* [2015] illustrates that two stable states occur at $D^* = 0.05$ (for the overwash-flat) and $D^* = 1 - 0.8$ (for resistant-dune)—values which are effectively identical to those presented here (Figures 3 and 5).

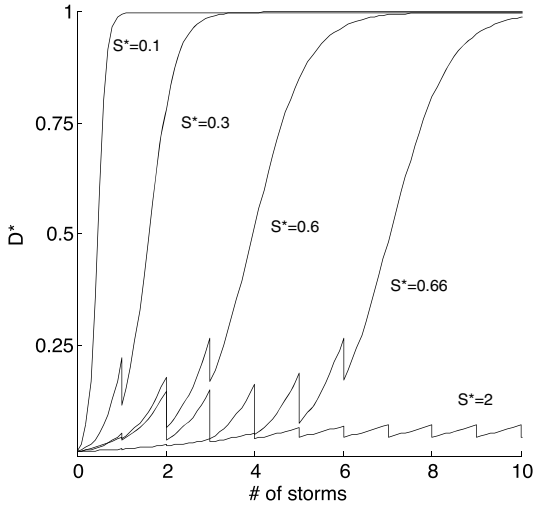

Figure 7. Nondimensional dune height time series (threshold model) for $R^* = 0.4$ and a values of S^* ranging from 0.1 to 2. Note $S^* = 2$ is the only value in the bistable region. Trajectories are affected as S^* approaches the bifurcation, which occurs at $S^* \cong 0.68$.

Durán and Moore [2015] demonstrate that the transition from a single stable state (resistant-dunes) to bistability is brought about by an increase in a "vulnerability index," which captures the competition between factors that build dunes and factors that erode dunes. Parsing the vulnerability index reveals that bistability is likely to occur when storm frequency is high, vegetation is particularly sensitive to salt water stress or grows slowly, aeolian sand flux is low, and/or the rate of relative sea level rise is high. One key related result from the model we present here is that when $R^* > 0.1$, a fold bifurcation occurs in all models as a result of variation in S^* only (see Figures 3–5). For example, using the basic model presented in (8), when $R^* = 0.1$ the bifurcation occurs at

$S^* = 0.75$, compared to $S^* = 0.61$ when $R^* = 1$ (Figure 3). Because the onset for bifurcation occurs within a narrow range of $S^*(0.61 \leq S^* \leq 0.75)$, the transition from stable high island to a bistable region of phase space is primarily dependent only on a high storm frequency and/or a low intrinsic growth rate of dunes (a result of weak aeolian transport and/or vegetation sensitivity salt water). Thus, the exploratory model we present and the model of *Durán and Moore* [2015] are consistent with one another and show effectively identical results. Though the model of *Durán and Moore* [2015] is more flexible, incorporating more effects at smaller scales and a probabilistic representation of storm activity, the intentionally simplified model presented here demonstrates that the behaviors identified by *Durán and Moore* [2015] can be produced using a reduced set of equations and tunable parameters derived empirically. This simplified, exploratory model also allows us to unpack additional dynamics such as the bottleneck/ghost phenomenon, which may be discernable in observational time series.

The stability diagrams presented in this contribution can also be understood in the context of the conceptual model of *Stallins and Parker* [2003] and *Stallins* [2005], which was further developed by *Wolner et al*. [2013]. These investigations suggest that species-specific feedbacks and physical factors such as shell lag [*Wolner et al*., 2013] can promote the development of disturbance resistant or disturbance reinforcing topography, similar to the two attracting states presented here (resistant-dune and overwash-flat) and the two attracting states presented by *Durán and Moore* [2015] (high and low). Note that although *Stallins and Parker* [2003], *Stallins* [2005], *Wolner et al*. [2013], and *Brantley et al*. [2014] do not address these end-members as alternate stable states, they do consider the additional, potential role of species-specific vegetation feedbacks. Though we do not explicitly address these feedbacks in this work, they can be understood in the context of the model we present; dune-building vegetation may have different efficacy in slowing wind, trapping sand, and/or vertical growth—all reducible, for the sake of this model, to adjustments in the intrinsic growth rate of dunes (r). This in turn will change model values of S^* and impact the region of phase space (and the number of permissible attracting states) for a given system.

4.2. Comparison to Observations

We assemble data from observational studies conducted along the U.S. East Coast to investigate the explanatory power of our model. There are several temporal signals that serve as evidence to suggest that our model is capturing the dynamics of coastal dunes. The most straightforward is the persistence of high resistant-dunes and/or low overwash-flats; observed persistence of these states would suggest that the attracting states arising in this model are present in nature. The presence of both stable states in the same geographic location (and under identical forcing conditions) would also be suggestive of the bistable dynamics arising from our model.

We find several observational studies that describe the temporal persistence of high resistant-dunes and low overwash-flats, identical to the behavior predicted in our model. Stable high dunes are found by *Stallins and Parker* [2003] on Sapelo Island, Georgia, where the last hurricane strike was 1979 [*Bossak et al*., 2014]. *Hosier and Cleary* [1977] study repeat aerial photography of Masonboro Island, North Carolina, spanning 27 years. Their analysis suggests that areas of Masonboro Island tend to be persistently overwashed in sequential storm events, consistent with model behavior presented here (i.e., that the low overwash-flat state is an attracting state). Further, *Hosier and Cleary* [1977] also describe areas of Masonboro Island in which high dunes (4 m) persist regardless of repeat storm events. This is consistent with the resistant-dune attracting state in our model, for the case in which dune growth is able to outcompete storm erosion. *Cleary and Hosier* [1979] extend their earlier analysis of Masonboro Island to the entire southern North Carolina shoreline (17 islands, 237 km), presenting evidence that foredunes at other sites include a mix of low (overwash-flat) or high (resistant-dunes) found on Masonboro Island. The presence of both states on a single island is consistent our model results that suggest the presence of a bistable region of phase space.

Persistently overwashed sites also exist in other geographic locations. *Godfrey and Godfrey* [1973] and *Dolan* [1973] present evidence of repeat overwash from the southern Outer Banks of North Carolina. *Dolan* [1973] compiles five written historic accounts from 1885 to 1942 suggesting that storm surge and overwash was a regular process on these low islands. *Godfrey et al*. [1979] discuss the possibility for sites of overwash to develop into higher dunes or persist as low washover fans, depending on storm recurrence time and vegetation effects. Other scattered accounts of persistent overwash exist as well: *Leatherman and Zaremba* [1987] remark on washover flats of various sizes on Nauset Spit, Massachusetts, that tend to be overwashed during subsequent storms. *Wolner et al*. [2013] describes sites of persistent overwash on Metompkin Island, Virginia,

observed in historic aerial photos and during field campaigns. *Schupp et al*. [2013] summarized 20 years of data from Assateague Island, Maryland, where overwash occurred in specific regions of the island with a frequently of up to 20 times per year.

In addition to accounts of persistent overwash-flats or stable resistant-dunes, observations also exist of overwashed sites developing into mature foredunes. *Hosier and Cleary* [1977] describe several overwash areas on Masonboro Island, NC, that recover by building incipient foredunes between storm events. This is consistent with the interstorm growth dynamic of the model and the large basin of attraction for resistant-dunes (compared to overwash-flats). *Mathew et al*. [2010] and *Ollerhead et al*. [2013] present nearly a century of observation of coastal dunes in Prince Edward Island, Canada. After a significant overwash event where dunes were destroyed, complete rebuilding of the foredune took place [*Mathew et al*., 2010; *Ollerhead et al*., 2013]. *Wolner et al*. [2013] also report stratigraphic data (from coring and ground penetrating radar) on Hog Island, Virginia, that indicates former sites of overwash were able to recover into high dunes.

The transition from one state to another can also be illustrated by observations of behavior before and after anthropogenic modifications. Prior to the building of the dune line on the Outer Banks of North Carolina, U.S., the barrier islands were described as low, flat overwash prone regions [*Godfrey and Godfrey*, 1973; *Dolan*, 1973]. Since the construction of a continuous, high (~10 m) dune on the northern islands, built by the Civilian Conservation Corps, this region has been less prone to overwash and dunes remain in a high state in some locations for extended periods of time [*Godfrey and Godfrey*, 1973; *Dolan*, 1973]. This suggests that high resistant-dunes are an additional attracting state (the system is in the bistable region of phase space) and anthropogenic construction of dunes in areas of persistent overwash instantaneously changes the system from low overwash-flats attracting state to the high resistant-dune state.

Similar behavior has been observed along the northern end of Assateague Island where dunes were artificially constructed in former regions of persistent overwash [*Schupp et al*., 2013, and references therein]; overwash conditions did not become reestablished until the dunes were artificially deconstructed several years later to achieve National Park Service management goals [*Schupp et al*., 2013]. This example suggests that high resistant-dunes and low overwash-flats are both stable states, and that Assateague Island is likely located in the bistable region of phase space. This conforms with previous work by *Durán and Moore* [2015] who presented a bimodal histogram of foredune elevation from the Virginia Barrier Islands, U.S. (directly south of Assateague Island), broadly consistent with the idea that this geographic region is in the bistable region of phase space.

4.3. Possible Model Tests

The goal of this work is to provide a simplified model of coastal foredune dynamics to develop dynamical insight. Thus far, we have presented evidence from the literature indicating the persistence of overwash-flats and resistant-dunes, behavior that is consistent with model output (i.e., these can both be attracting states given the appropriate conditions). The simplified nature of this one-dimensional model inhibits straightforward, direct comparison with nature, primarily because of the use of a characteristic storm to simplify model behavior for maximum insight. However, we can envision observational studies that might serve as critical tests of the model. For example, the constituent equations of (8) could be explicitly further tested via observations: Does the logistic model of dune growth put forward by *Houser et al*. [2015] describe dune growth in other geographic regions? Does the highly simplified storm erosion model put forward here, using data from *Long et al*. [2014], describe dune erosion for other storms at other locations? Further, the model itself could be tested. For example, a time series of foredune height (at a given location) coupled with a record of total water level could be used as initial conditions and forcing for the model, respectively. The observational time series of dune height could then be compared to the modeled dune height time series. Conducting this test would also require several critical parameters to be determined empirically for the study site (i.e., r and D_{max}). Future work will focus on testing the model and the constituent equations, as well as linking this model framework to more complex probabilistic storm climate [e.g., *Serafin and Ruggiero*, 2014].

4.4. Concluding Remarks

In this contribution we develop a one-dimensional model for coastal foredune height by combing an equation for interstorm dune growth with an equation for dune erosion by storm events. We find that two stable attracting states exist: a high resistant-dune state and a low overwash-flat state. Within a defined region of phase

space the model is bistable—both states are stable. Our findings are consistent with previous model results and many observations of island state along the U.S. Atlantic coast.

Our parameterization for dune erosion during storm events is derived directly from data fed through a machine learning technique to extract a smooth relationship. Coupling theoretical components (3a) with machine learning parameterizations (3b) in this way is an example of a "hybrid" model [e.g., *Krasnopolsky and Fox-Rabinovitz*, 2006; *Goldstein and Coco*, 2015]. This contribution serves as a further example of the utility in using machine learning processes for constructing models of coastal environments [e.g., *Goldstein et al.*, 2014; *Limber et al.*, 2014].

Lastly, many coastal dune systems are heavily managed [e.g., *Nordstrom*, 2000]. Understanding the location of the separatrix, the height that separates the basin of attraction for higher resistant-dune and lower overwash-flat states is potentially useful for dune rehabilitation projects, specifically projects that intend to restore dunes in a natural manner by allowing them to build slowly [*Nordstrom*, 2008].

Acknowledgments
We thank P. W. Limber, A. B. Murray, K. M. Ratliff, and R. Lauzon for their valuable suggestions during this study. We thank V. Voller, A. Ashton, and two anonymous reviewers for their comments on an earlier version of the manuscript. We thank three additional anonymous reviewers, the Associate Editor, and the Editor for their valuable constructive feedback on this manuscript. Model code used in this paper is available on the website of EBG. Funding was provided by NSF-GLD (EAR-1324973).

References

Arens, S. M. (1996), Patterns of sand transport on vegetated foredunes, *Geomorphology*, *17*, 339–350.
Arens, S. M., A. C. W. Baas, J. H. van Boxel, and C. Kalkman (2001), Influence of reed stem density on foredune development, *Earth Surf. Processes Landforms*, *26*, 176.
Bainov, B., and P. Simeonov (1993), *Impulsive Differential Equations: Periodic Solutions and Applications*, *Pitman Monogr. Surveys Pure Appl. Math.*, vol. 66, Longman, Harlow.
Bauer, B. O., and R. G. D. Davidson-Arnott (2002), A general framework for modeling sediment supply to coastal dunes including wind angle, beach geometry, and fetch effects, *Geomorphology*, *49*(1–2), 89–108.
Bauer, B. O., R. G. D. Davidson-Arnott, I. J. Walker, P. A. Hesp, and J. Ollerhead (2012), Wind direction and complex sediment transport response across a beach–dune system, *Earth Surf. Process. Landforms*, *37*, 1661–1677, doi:10.1002/esp.3306.
Bel, G., and Y. Ashkenazy (2014), The effects of psammophilous plants on sand dune dynamics, *J. Geophys. Res. Earth Surf.*, *119*, 1636–1650, doi:10.1002/2014JF003170.
Bossak, B. H., S. S. Keihany, M. R. Welford, and E. J. Gibney (2014), Coastal Georgia Is Not Immune: Hurricane History, 1851–2012, *Southeast. Geogr.*, *54.3*(2014), 323–333.
Brantley, S. T., S. N. Bissett, D. R. Young, C. W. Wolner, and L. J. Moore (2014), Barrier island morphology and sediment characteristics affect the recovery of dune building grasses following storm-induced overwash, *PLoS One*, *29*(8), e104747.
Carr, J., P. D'Odorico, K. McGlathery, and P. Wiberg, (2010), Stability and bistability of seagrass ecosystems in shallow coastal lagoons: Role of feedbacks with sediment resuspension and light attenuation, *J. Geophys. Res.*, *115*, G03011, doi:10.1029/2009JG001103.
Claudino-Sales, V., P. Wang, and M. H. Horwitz (2008), Factors controlling the survival of coastal dunes during multiple hurricane impacts in 2004 and 2005: Santa Rosa barrier island, Florida, *Geomorphology*, *95*, 295–315.
Cleary, W. J., and P. E. Hosier (1979), Geomorphology, washover history, and inlet zonation: Cape Lookout, NC to Bird Island, NC, in *Barrier Islands: From the Gulf of St. Lawrence to the Gulf of Mexico*, edited by S. P. Leatherman, pp. 237–269, Academic Press, New York.
Coco, G., S. Thrush, M. Green, and J. Hewitt (2006), Feedbacks between bivalve density, flow, and suspended sediment concentration on patch stable states, *Ecology*, *87*(11), 2862–2870.
de Vries, S., H. Southgate, W. Kanning, and R. Ranasinghe (2012), Dune behavior and aeolian transport on decadal timescales, *Coastal Eng.*, *67*, 41–53.
Dolan, R. (1973), Barrier islands: Natural and controlled, in *Coastal Geomorphology*, edited by D. R. Coates, pp. 239–257, State University, New York.
Durán, O., and L. J. Moore (2013), Vegetation controls on the maximum size of coastal dunes, *Proc. Natl. Acad. Sci. U.S.A.*, doi:10.1073/pnas.1307580110.
Durán, O., and L. J. Moore (2015), Barrier island bistability induced by biophysical interactions, *Nat. Clim. Change*, 1758–6798, doi:10.1038/nclimate2474.
Emanuel, K. A. (2013), Downscaling CMIP5 climate models shows increased tropical cyclone activity over the 21st century, *Proc. Natl. Acad. Sci. U.S.A.*, *110*, 12,219–12,224, doi:10.1073/pnas.1301293110.
Fagherazzi, S., L. Carniello, L. D'Alpaos, and A. Defina (2006), Critical bifurcation of shal- low microtidal landforms in tidal flats and salt marshes, *Proc. Natl. Acad. Sci. U.S.A.*, *103*, 8,337–8,341, doi:10.1073/pnas.0508379103.
Godfrey, P. J., and M. M. Godfrey (1973), Comparison of ecological and geomorphic interactions between aldered and unaldered barrier island systems in North Carolina, in *Coastal Geomorphology*, edited by D. R. Coates, pp. 239–257, State University, New York.
Godfrey, P. J., S. P. Leatherman, and R. Zaremba (1979), A geobotanical approach to classification of barrier beach systems, in *Barrier islands: From the Gulf of St. Lawrence to the Gulf of Mexico*, edited by S. P. Leatherman, pp. 99–126, Academic Press, New York.
Goldstein, E. B., and G. Coco (2015), Machine learning components in deterministic models: Hybrid synergy in the age of data, *Front. Environ. Sci.*, *3*, 33, doi:10.3389/fenvs.2015.00033.
Goldstein, E. B., G. Coco, and A. B. Murray (2013), Prediction of wave ripple characteristics using genetic programming, *Cont. Shelf Res.*, *71*, 1–15, doi:10.1016/j.csr.2013.09.020.
Goldstein, E. B., G. Coco, A. B. Murray, and M. O. Green (2014), Data-driven components in a model of inner-shelf sorted bedforms: A new hybrid model, *Earth Surf. Dynam.*, *2*, 67–82, doi:10.5194/esurf-2-67-2014.
Hacker, S. D., P. Zarnetske, E. Seabloom, P. Ruggiero, J. Mull, S. Gerrity, and C. Jones (2012), Subtle differences in two non-native congeneric beach grasses significantly affect their colonization, spread, and impact, *Oikos*, *121*, 138–148.
Heffernan, J. B. (2008), Wetlands as an alternative stable state in desert streams, *Ecology*, *89*, 1261–1271.
Hesp, P. A. (1989), A review of biological and geomorphological processes involved in the initiation and development of incipient foredunes, in *Coastal Sand Dunes*, vol. 96B, edited by C. H. Gimingham et al., pp. 181–201, Proceedings of Royal Society, Edinburgh.
Hesp, P. A. (2002), Foredunes and blowouts: Initiation, geomorphology and dynamics, *Geomorphology*, *48*, 245–268.

Hesp, P. A. (2004), Coastal dunes in the tropics and temperate regions: location, formation, morphology and vegetation processes, in *Coastal Dunes: Ecology and Conservation, Ecological Studies*, vol. 171, edited by M. L. Martínez and N. P. Psuty, pp. 29–49, Springer-Verlag, Berlin.
Hosier, P. E., and W. J. Cleary (1977), Cyclic geomorphic patterns of washover on a barrier island in southeastern NC, *Environ. Geol.*, *2*(2), 23–31.
Houser, C., and S. Hamilton (2009), Sensitivity of post-hurricane beach and dune recovery to event frequency, *Earth Surf. Processes Landforms*, *34*, 613–628, doi:10.1002/esp.1730.
Houser, C., P. Wernette, E. Rentschlar, H. Jones, B. Hammond, and S. Trimble (2015), Post-storm beach and dune recovery: Implications for barrier island resilience, *Geomorphology*, *234*(1), 54–63, doi:10.1016/j.geomorph.2014.12.044.
Intergovernmental Panel on Climate Change (2014), *Climate Change 2014: Impacts, Adaptation and Vulnerability: Contributions of Working Group II to the Fifth Assessment Report of the Intergovernmental Panel on Climate Change*, Cambridge Univ. Press, New York.
Keijsers J. G. S., A. Poortinga, M. J. P. M. Riksen, and J. Maroulis (2014), Spatio-temporal variability in accretion and erosion of coastal foredunes in the Netherlands: Regional climate and local topography, *PLoS One*, *9*(3), e91115, doi:10.1371/journal.pone.0091115
Keijsers, J. G. S., A. V. De Groot, and M. J. P. M. Riksen (2015), Vegetation and sedimentation on coastal foredunes, *Geomorphology*, *228*, 723–734, doi:10.1016/j.geomorph.2014.10.027.
Kinast, S., E. Meron, H. Yizhaq, and Y. Ashkenazy (2013), Biogenic crust dynamics on sand dunes, *Phys. Rev. E*, *87*, 020701(R), doi:10.1103/PhysRevE.87.020701.
Koza, J. R. (1992), *Genetic Programming, on the Programming of Computers by Means of Natural Selection*, MIT Press, Cambridge, Mass.
Krasnopolsky, V. M., and M. S. Fox-Rabinovitz (2006), A new synergetic paradigm in environmental numerical modeling: Hybrid models combining deterministic and machine learning components, *Ecol. Model.*, *191*, 5–18.
Kuriyama, Y., N. Mochizuki, and N. Tsuyoshi (2005), Influence of vegetation on aeolian sand transport rate from a backshore to a foredune at Hasaki, Japan, *Sedimentology*, *52*(5), 1123–1132, doi:10.1111/j.1365-3091.2005.00734.x.
Leatherman, S. P., and R. E. Zaremba (1987), Overwash and aeolian processes on a U.S. northeast coast barrier, *Sediment. Geol.*, *52*, 183–206.
Limber, P. W., A. B. Murray, P. N. Adams, and E. B. Goldstein (2014), Unraveling the dynamics that scale cross-shore headland relief on rocky coastlines: 1. Model development, *J. Geophys. Res. Earth Surf.*, *119*, 854–873, doi:10.1002/2013JF002950.
Long, J. W., A. T. M. de Bakker, and N. G. Plant (2014), Scaling coastal dune elevation changes across storm-impact regimes, *Geophys. Res. Lett.*, *41*, 2899–2906, doi:10.1002/2014GL059616.
Marani, M., A. D'Alpaos, S. Lanzoni, L. Carniello, and A. Rinaldo (2010), The importance of being coupled: Stable states and catastrophic shifts in tidal biomorphodynamics, *J. Geophys. Res.*, *115*, F04004, doi:10.1029/2009JF001600.
Mathew, S., R. G. D. Davidson-Arnott, and J. Ollerhead (2010), Evolution of a beach/dune system following overwash during a catastrophic storm: Greenwich Dunes, Prince Edward Island, 1936–2005, *Can. J. Earth Sci.*, *47*, 273–290.
Maun, A., and J. Perumal (1999), Zonation of vegetation on lacustrine coastal dunes: Effects of burial by sand, *Ecol. Lett.*, *2*, 14–18.
McCall, R., J. Van Thiel de Vries, N. Plant, A. Van Dongeren, J. Roelvink, D. Thompson, and A. Reniers (2010), Two-dimensional time dependent hurricane overwash and erosion modeling at Santa Rosa Island, *Coastal Eng.*, *57*(7), 668–683.
McLean, R., and J. S. Shen (2006), From foreshore to foredune: Foredune development over the last 30 years at Moruya Beach, New South Wales, *J. Coast. Res.*, *22*, 28–36.
Morton, R. A., J. G. Paine, and J. C. Gibeaut (1994), Stages and durations of post-storm beach recovery, southeastern Texas coast, USA, *J. Coast. Res.*, *10*(4), 884–908.
Murray, A. B. (2003), Contrasting the goals, strategies, and predictions associated with simplified numerical models and detailed simulations, in *Prediction in Geomorphology*, *AGU Geophysical Monograph*, vol. 135, edited by R. M. Iverson and P. R. Wilcock, pp. 151–165, AGU, Washington, D. C.
Nordstrom, K. F. (2000), *Beaches and Dunes on Developed Coasts*, pp. 338, Cambridge Univ. Press, Cambridge, U. K.
Nordstrom, K. F. (2008), *Beaches and Dunes Restoration*, pp. 200, Cambridge Univ. Press, Cambridge, U. K.
Ollerhead, J., R. G. D. Davidson-Arnott, I. J. Walker, and S. Mathew (2013), Annual to decadal morphodynamics of the foredune system at Greenwich Dunes, Prince Edward Island, Canada, *Earth Surf. Processes Landforms*, *38*, 284–298.
Palmsten, M. L., and R. A. Holman (2011), Infiltration and instability in dune erosion, *J. Geophys. Res.*, *116*, C10030, doi:10.1029/2011JC007083.
Ryu, W., and D. J. Sherman (2014), Foredune texture: Landscape metrics and climate, *Ann. Assoc. Am. Geogr.*, *104*, 903–921.
Sallenger, A. H., Jr. (2000), Storm impact scale for barrier islands, *J. Coast. Res.*, *16*(3), 890–895.
Scheffer, M., J. Bascompte, W. A. Brock, V. Brovkin, S. R. Carpenter, V. Dakos, H. Held, E. H. van Nes, M. Rietkerk, and G. Sugihara (2009), Early-warning signals for critical transitions, *Nature*, *461*, 53–59.
Schmidt, M., and H. Lipson (2009), Distilling free-form natural laws from experimental data, *Science*, *324*, 81–85.
Schmidt, M., and H. Lipson (2014), Eureqa (Version 0.98 beta) [Software], [Available at http://www.eureqa.com/.]
Schupp, C. A., N. T. Winn, T. L. Pearl, J. P. Kumer, T. J. B. Carruthers, and C. S. Zimmerman (2013), Restoration of overwash processes creates piping plover (Charadrius melodus) habitat on a barrier island (Assateague Island, Maryland), *Estuarine Coastal Shelf Sci.*, *116*, 11–20.
Serafin, K. A., and P. Ruggiero (2014), Simulating extreme total water levels using a time-dependent, extreme value approach, *J. Geophys. Res. Oceans*, *119*, 6305–6329, doi:10.1002/2014JC010093.
Stallins, J. A. (2005), Stability domains in barrier island dune systems, *Ecol. Complex.*, *2*, 410–430.
Stallins, J. A., and A. J. Parker (2003), The influence of complex systems interactions on barrier island dune vegetation pattern and process, *Ann. Assoc. Am. Geogr.*, *93*(1), 13–29.
Strogatz, S. H. (2001), *Nonlinear Dynamics and Chaos—With Applications to Physics, Biology, Chemistry and Engineering*, pp. 498, Westview Press, New York.
Tang, S., and L. Chen (2002), Density-dependent birth rate, birth pulses and their population dynamic consequences, *J. Math. Biol.*, *44*, 185–199.
Tebaldi, C., C. E. Zervas, and B. H. Strauss (2012), Modelling sea level rise impacts on storm surges along US coasts, *Environ. Res. Lett.*, *7*, 014032
Tinoco, R. O., E. B. Goldstein, and G. Coco (2015), A data-driven approach to develop physically sound predictors: Application to depth- averaged velocities on flows through submerged arrays of rigid cylinders, *Water Resour. Res.*, *51*, 1247–1263, doi:10.1002/2014WR016380.
Verhulst, P. F. (1838), Notice sur la loi que la population suit dans son accroissement, *Corresp. Math. Phys.*, *10*, 113–121.
Wolner, C. W. V., L. J. Moore, D. R. Young, S. T. Brantley, S. N. Bissett, and R. A. McBride (2013), Ecomorphodynamic feedbacks and barrier island response to disturbance: Insights from the Virginia Barrier Islands, Mid-Atlantic Bight, USA, *Geomorphology*, *199*, 115–128.
Yizahq, H., Y. Ashkenazy, and H. Tsoar (2007), Why do active and stabilized dunes coexist under the same climatic conditions?, *Phys. Rev. Lett.*, *98*, 188001.
Yizahq, H., Y. Ashkenazy, and H. Tsoar (2009), Sand dune dynamics and climate change: A modeling approach, *J. Geophys. Res.*, *114*, F01023, doi:10.1029/2008JF001138.
Zarnetske, P. L., S. D. Hacker, E. W. Seabloom, P. Ruggiero, J. R. Killian, T. B. Maddux, and D. Cox (2012), Biophysical feedback mediates effects of invasive grasses on coastal dune shape, *Ecology*, *93*, 1439–1450.